

Observation of topological transitions in interacting quantum circuits

P. Roushan^{1†*}, C. Neill^{1*}, Yu Chen^{1†*}, M. Kolodrubetz², C. Quintana¹, N. Leung¹, M. Fang¹, R. Barends^{1†}, B. Campbell¹, Z. Chen¹, B. Chiaro¹, A. Dunsworth¹, E. Jeffrey^{1†}, J. Kelly¹, A. Megrant¹, J. Mutus^{1†}, P. J. J. O'Malley¹, D. Sank^{1†}, A. Vainsencher¹, J. Wenner¹, T. White¹, A. Polkovnikov², A. N. Cleland¹ & J. M. Martinis^{1,3}

Topology, with its abstract mathematical constructs, often manifests itself in physics and has a pivotal role in our understanding of natural phenomena. Notably, the discovery of topological phases in condensed-matter systems has changed the modern conception of phases of matter^{1–5}. The global nature of topological ordering, however, makes direct experimental probing an outstanding challenge. Present experimental tools are mainly indirect and, as a result, are inadequate for studying the topology of physical systems at a fundamental level. Here we employ the exquisite control afforded by state-of-the-art superconducting quantum circuits to investigate topological properties of various quantum systems. The essence of our approach is to infer geometric curvature by measuring the deflection of quantum trajectories in the curved space of the Hamiltonian⁶. Topological properties are then revealed by integrating the curvature over closed surfaces, a quantum analogue of the Gauss–Bonnet theorem. We benchmark our technique by investigating basic topological concepts of the historically important Haldane model⁷ after mapping the momentum space of this condensed-matter model to the parameter space of a single-qubit Hamiltonian. In addition to constructing the topological phase diagram, we are able to visualize the microscopic spin texture of the associated states and their evolution across a topological phase transition. Going beyond non-interacting systems, we demonstrate the power of our method by studying topology in an interacting quantum system. This required a new qubit architecture^{8,9} that allows for simultaneous control over every term in a two-qubit Hamiltonian. By exploring the parameter space of this Hamiltonian, we discover the emergence of an interaction-induced topological phase. Our work establishes a powerful, generalizable experimental platform to study topological phenomena in quantum systems.

Since the first observations of topological ordering in quantum Hall systems in the 1980s^{1,2}, experimental studies of topological phases have mainly been performed with a limited number of primarily indirect measurement techniques. For instance, transport measurements are the predominant tool used to study the quantum Hall effect, where interpretations¹⁰ are required to infer topological properties from the measurements. Consequently, topological studies in quantum systems where transport measurements cannot be carried out have remained elusive.

In principle, topological properties can be explored in any quantum system where the Hamiltonian can be written in terms of a set of parameters. Topological phases are characterized by topological invariants, such as the first Chern number $\mathcal{C}\mathcal{H}$, whose discrete jumps indicate transitions between different topologically ordered phases^{11,12}. For a quantum system, $\mathcal{C}\mathcal{H}$ is defined as the integral over a closed manifold \mathcal{S} in the parameter space of the Hamiltonian as

$$\mathcal{C}\mathcal{H} \equiv \frac{1}{2\pi} \oint_{\mathcal{S}} \mathbf{B} \cdot d\mathbf{S} \quad (1)$$

where \mathbf{B} is the vector form of the Berry curvature¹³. As illustrated in Fig. 1 and shown in Supplementary Information, \mathbf{B} can be viewed as an

effective magnetic field with points of ground-state degeneracy acting as its sources, that is, magnetic monopoles¹⁴. Using Gauss's law for the Berry curvature (magnetic field), $\mathcal{C}\mathcal{H}$ simply counts the number of degenerate energy eigenvalues (magnetic monopoles) enclosed by the parameter manifold \mathcal{S} . $\mathcal{C}\mathcal{H}$, which is invariant under perturbations to the shape of \mathcal{S} , is a topological number that reflects a property of the manifold of states as a whole and not a local property of parameter space.

In previous works, topological properties of highly symmetric quantum systems have been measured^{15–17}. However, since these earlier studies relied on interference, these methods are not readily generalizable. To circumvent this, Gritsev *et al.*⁶ proposed a general method to directly measure the local Berry curvature. The underlying physics of their idea is that motion in a curved space will be deflected from a straight trajectory; in other words, curvature reveals itself as an effective force, analogous to a charged particle moving in a magnetic field experiencing the well-known Lorentz force. Similarly, Gritsev *et al.* showed that in a region of the parameter space with Berry curvature \mathbf{B} , if we 'move' a quantum system by changing a parameter of its Hamiltonian with rate $|\mathbf{v}|$, then the state of the system feels a force \mathbf{F} given by

$$\mathbf{F} \propto \mathbf{v} \times \mathbf{B} + \mathbf{O}(\mathbf{v}^2), \quad (2)$$

where \mathbf{O} indicates higher-order terms. This force leads to deviations of the trajectory from the adiabatic path, which can be detected through measurements of the observables of the system (Fig. 1). As long as the

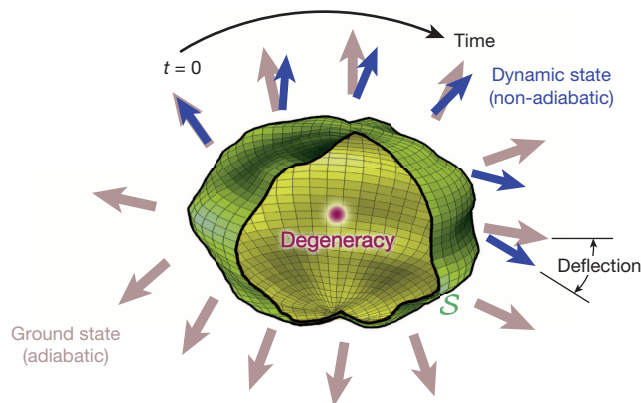


Figure 1 | Dynamical measurement of Berry curvature and $\mathcal{C}\mathcal{H}$. In this schematic drawing, brown arrows represent the ground states (adiabatic limit) for given points on a closed manifold \mathcal{S} (green enclosure, interrupted by an opening for the sake of illustration) in the Hamiltonian's parameter space, and the blue arrows are the measured states during a non-adiabatic passage. According to equation (2) in the main text, the Berry curvature \mathbf{B} can be calculated from the deflection from adiabaticity. Integrating \mathbf{B} over \mathcal{S} gives the Chern number $\mathcal{C}\mathcal{H}$, which corresponds to the total number of degeneracy points (such as the brown point) enclosed.

¹Department of Physics, University of California, Santa Barbara, California 93106-9530, USA. ²Department of Physics, Boston University, Boston, Massachusetts 02215, USA. ³Google Inc., Santa Barbara, California 93117, USA. †Present address: Google Inc., Santa Barbara, California 93117, USA.

*These authors contributed equally to this work.

ramping of parameters is done slowly, but not necessarily adiabatically, the deviation is directly proportional to \mathbf{B} . Since the adiabatic limit is generally hard to achieve, this relation has the important advantage of needing only a moderately slow change of state and only requires that the linear term dominates the response.

Direct measurement of \mathbf{B} provides an alternative means to study topological phases that differs significantly from conventional approaches. In condensed-matter systems an instantaneous realization of the entire phase space manifold, such as the Fermi surface, is required. In our approach, the local curvature of the space is dynamically ‘sensed’ and topological invariants, such as $\mathcal{C}\mathcal{H}$, are inferred by integrating these measurements. Implementing this dynamical procedure requires the ability to continuously change the system Hamiltonian. In fully controllable quantum systems, where this can be achieved, this method provides a powerful means to probe topological properties.

To elucidate this dynamical method, we demonstrate a basic implementation in quantum circuits with superconducting qubits^{18–20}. The quantum state of a single qubit²¹ is equivalent to a spin-1/2 particle in a magnetic field. Its Hamiltonian in the rotating frame can be written as

$$\mathcal{H}_S = -\frac{\hbar}{2} \mathbf{H} \cdot \boldsymbol{\sigma}, \quad (3)$$

where $\boldsymbol{\sigma} = (\sigma^x, \sigma^y, \sigma^z)$ are the Pauli matrices, and $\mathbf{H} = (H_x, H_y, H_z)$ is analogous to a control magnetic field. Full control over the parameters of this Hamiltonian is achieved by microwave pulses that control H_x and H_y , and an applied flux through the qubit’s SQUID (superconducting quantum interference device) loop which controls H_z . We measure $\mathcal{C}\mathcal{H}$ for spherical ground-state manifolds in \mathbf{H} parameter space (Fig. 2). We use θ and ϕ as spherical coordinates and consider the parameter trajectory that starts at the north pole at $t = 0$ and ramps along the $\phi = 0$ meridian ($H_y = 0$) with constant velocity $v_\theta = d\theta/dt$ until it reaches the south pole at final time $t = T_f$. To realize motion on a spherical manifold, the control sequences of H_z and H_x are chosen such that the control magnitude $|\mathbf{H}| = H_r$ is constant. In the adiabatic limit, the wavefunction would remain in the instantaneous ground state of \mathcal{H}_S , that is, the $\phi = 0$ meridian on the Bloch sphere. For non-adiabatic ramps, instead, a deviation from the meridian is observed, as shown in Fig. 2b. Here the Bloch vector is measured at each point in time by interrupting the ramp and performing state tomography. Note that this deviation is not due to noise, but rather is the expected non-adiabatic response due to local Berry curvature. For this trajectory, the force \mathbf{F} takes the form $f_\phi = \frac{\hbar}{2} H_r \langle \sigma^y \rangle \sin \theta$, and integrating over the resulting deflection (shaded light red in Fig. 2b) gives $\mathcal{C}\mathcal{H} = 1 \pm 0.05$. Given the symmetry of this Hamiltonian, a line integral is sufficient for measuring the surface integral of $\mathcal{C}\mathcal{H}$ (refs 22, 23). A value of unity is expected, as the qubit ground state has a degeneracy at $\mathbf{H} = 0$, corresponding to a single monopole enclosed by the parameter sphere \mathcal{S} . We demonstrate the robustness of $\mathcal{C}\mathcal{H}$ by deforming the surface manifold \mathcal{S} (see Supplementary Information).

The generality of our approach allows us to connect our measurements to certain condensed-matter systems and their core topological features, such as topological phase transitions and the geometric winding of state vectors. This can be done by establishing a mapping from the real or momentum space of the model condensed-matter system to the parameter space of the controllable quantum circuit. We choose what is perhaps the simplest theoretical model of topological behaviour, the Haldane model⁷, to benchmark our approach. This model serves as a foundation for other topological insulator models^{3–5}. To show that the quantum Hall effect could be achieved without a global magnetic field, Haldane introduced a non-interacting Hamiltonian⁷ given by

$$\mathcal{H}_G(k_x, k_y) = \hbar v_F (k_x \sigma^x + k_y \sigma^y) + (m_0 - m_t) \sigma^z \quad (4)$$

where v_F is the Fermi velocity, k_x, k_y are the (momentum-space) coordinates, m_0 is the effective mass, and m_t corresponds to a second-neighbour hopping (tunnelling) in a local magnetic field. The key prediction of the Haldane model is that if $m_0/m_t > 1$ the system is in a trivial insulating

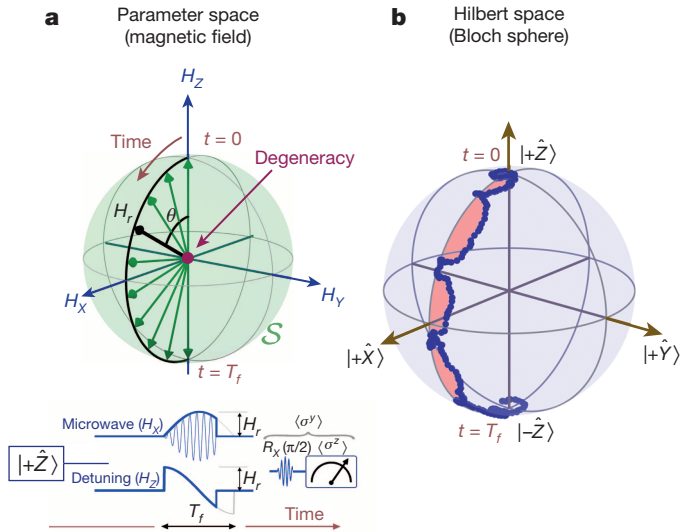


Figure 2 | Dynamical measurement of $\mathcal{C}\mathcal{H}$. **a**, A simultaneous microwave pulse $H_x(t) = H_r \sin(\pi t/T_f)$ and detuning pulse $H_z(t) = H_r \cos(\pi t/T_f)$ are applied to construct a parameter-space trajectory. The pulse sequence results in a parameter-space motion along the $\phi = 0$ meridian ($H_y = 0$ plane) on \mathcal{S} . The lower panel shows the pulse sequence applied to the system from preparation to measurement. **b**, The state of the qubit during this ramp ($H_r/2\pi = 10$ MHz and $T_f = 600$ ns) is determined using tomography, and shown (blue dots) on the surface of the Bloch sphere. The light red shading shows the deflection integrated over, yielding $\mathcal{C}\mathcal{H} = 1 \pm 0.05$.

phase, and otherwise in a topological phase. Using a confocal mapping (see Supplementary Information), one can recast equation (4) into the single-qubit Hamiltonian of equation (3). If we consider spherical manifolds \mathcal{S} of radius H_r displaced from the origin in the z direction by H_0 , then H_0/H_r in the qubit system plays the same role as m_0/m_t in the Haldane model.

In Fig. 3a we plot the results of this measurement, showing $\mathcal{C}\mathcal{H}$ as a function of H_r and H_0 , which shows plateaux at values 0 and 1 separated by a phase transition boundary line at $H_r = H_0$. This transition can be easily understood: when $H_0 < H_r$, the degeneracy at $\mathbf{H} = 0$ lies within \mathcal{S} giving $\mathcal{C}\mathcal{H} = 1$, whereas for $H_0 > H_r$, it lies outside \mathcal{S} giving $\mathcal{C}\mathcal{H} = 0$.

In the Haldane model, the topological and the trivial phase each has its own signature spin texture in momentum space. Microscopic structure of these phases can be revealed by the conventional adiabatic method. We again consider spherical surfaces \mathcal{S} and adiabatically ramp the control parameters to their final values on \mathcal{S} . The resulting Bloch vectors are then tomographically measured. With a confocal mapping (see Supplementary Information), \mathcal{S} can be mapped to the first Brillouin zone (FBZ) of the honeycomb lattice. Therefore, the adiabatically measured ground-state vectors on \mathcal{S} can be depicted in the FBZ. Figure 3b, c shows the results for two manifolds with $H_0/H_r = 1.2$ and 0, corresponding to trivial and topological phases, respectively. By following the orientation of the state-vector along any path starting at \mathbf{K} and moving to \mathbf{K}' (corners of the FBZ) and back to \mathbf{K} , one can see that in the topological case the state vector wraps around and makes one full rotation, while in the trivial case it only tilts away from vertical and then returns, without completing a rotation. These spin texture maps can also be used to extract local Berry curvature. As shown in Fig. 3c, the resulting $\mathcal{C}\mathcal{H}$ from this adiabatic method shows good agreement with the dynamical method of measurement.

Some of the most fascinating topological phenomena in quantum systems emerge in the presence of interaction. Compared to non-interacting systems, interactions impose a greater experimental challenge to studying topological properties. Nevertheless, the method outlined here stands out in its ability to provide insight into the topology of such systems. To illustrate this, we consider the most basic unit of interaction and measure $\mathcal{C}\mathcal{H}$ in a coupled two-qubit system. One major experimental challenge

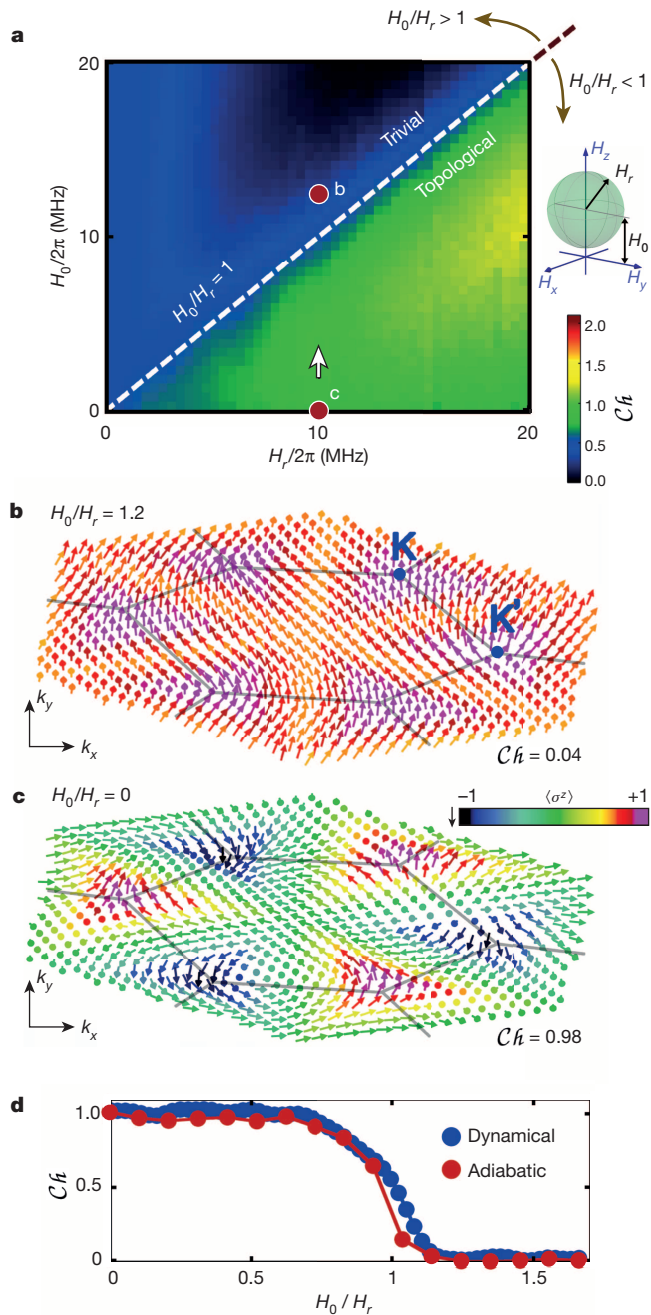


Figure 3 | Dynamic measurement of the topological phase diagram and adiabatic visualization of phases. **a**, Dynamical determination of the phase diagram. First $\langle \sigma^z \rangle$ was measured during ramps similar to those in Fig. 2a, and then $\mathcal{C}\hbar$ was calculated. The dashed line is the expected phase boundary at $H_0 = H_r$. The ramp speed was $T_f = 1,000$ ns. Red dots show locations of the states whose properties are shown in panels **b** and **c**. **b**, **c**, With adiabatic state preparation, the state of the qubit was prepared and measured over a grid on the surface of the parameter sphere and then mapped to the hexagonal momentum-space plane. The ground states are presented as Bloch vectors, whose colours indicate their $\langle \sigma^z \rangle$ values (see key). $H_0/H_r = 1.2$ for **b** and $H_0/H_r = 0$ for **c**. The grey lines show the FBZ of the honeycomb lattice and high symmetry points **K** and **K'** are marked. Each adiabatic sequence took $T_f = 1,000$ ns. **d**, The measured $\mathcal{C}\hbar$ from the adiabatic and dynamical (white arrow in **a**) methods are plotted versus H_0/H_r .

here is the need for full control over the entire parameter space of the Hamiltonian. Here we achieve this by using a new design for our superconducting qubits, which includes the ability to continuously vary the inter-qubit coupling strength g (refs 8, 9). The Hamiltonian of this system in a frame rotating with the qubits is given by

$$\mathcal{H}_{2Q} = -\frac{\hbar}{2} [H_0 \sigma_1^z + \mathbf{H}_1 \cdot \boldsymbol{\sigma}_1 + \mathbf{H}_2 \cdot \boldsymbol{\sigma}_2 - g(\sigma_1^x \sigma_2^x + \sigma_1^y \sigma_2^y)] \quad (5)$$

where 1 and 2 refer to qubit 1 (Q1) and qubit 2 (Q2), respectively, and the biasing field H_0 is now only applied to Q1. In this design, we can access all regions of the seven-dimensional parameter space of this Hamiltonian.

We explore spherical manifolds with fixed $(H_0, |\mathbf{H}_1|, |\mathbf{H}_2|, g)$, analogous to the single-qubit experiment. We perform experiments where both $\mathbf{H}_1 = \mathbf{H}_2 = \mathbf{H}_r$ are ramped simultaneously with magnitude $|\mathbf{H}_r| = H_r$ (Supplementary Information). The measured $\mathcal{C}\hbar$ is shown in Fig. 4a, c for three distinct cuts through this parameter space.

We begin in Fig. 4a by exploring the simplest case, $g = 0$, where the qubits behave independently and the physics can be understood using the single qubit results. Since only Q1 is subject to H_0 , its $\mathcal{C}\hbar$ changes by 1 through the transition $H_0 = H_r$. In contrast, in the absence of a biasing field, $\mathcal{C}\hbar$ of Q2 remains equal to 1. As the qubits are independent, the $\mathcal{C}\hbar$ of the system is simply the summation of the individual $\mathcal{C}\hbar$, leading to two phases with $\mathcal{C}\hbar = 1$ and $\mathcal{C}\hbar = 2$.

With the non-interacting limit of our system understood, we now focus on the effects of interaction by examining regions of parameter space where $g \neq 0$. Considering manifolds with constant $g/2\pi = 4$ MHz, we observe a new phase with $\mathcal{C}\hbar = 0$ (blue) when $H_r \lesssim g$, as shown in Fig. 4a. To gain more insight into this new phase, we continuously vary g and examine the evolution of the $\mathcal{C}\hbar = 0$ region. As shown in Fig. 4c, this phase appears when $g \approx H_r$, and monotonically expands as g increases. These observations and the fact that this phase is absent when $g = 0$ indicate that the $\mathcal{C}\hbar = 0$ phase is indeed driven by interaction.

In certain limits, the three phases could approximately be characterized by the dominance of the global field ($\mathcal{C}\hbar = 2$), of local fields (disorder; $\mathcal{C}\hbar = 1$), and of interaction ($\mathcal{C}\hbar = 0$). Interestingly, they also show some signature entanglement entropies (see Supplementary Information). The linear entropy of the states, averaged over the manifold, qualitatively hints towards a similar phase diagram in certain regions, where the phase with lowest $\mathcal{C}\hbar$ appears when the highest entanglement allowed in the system has been reached. However, since $\mathcal{C}\hbar$ is a global property, information about it cannot be deduced from the nature of any single ground state. The interplay of fields and interactions provides hints to anticipate the various topological phases in this system, but are incapable of capturing the entire underlying physics that leads to quantized $\mathcal{C}\hbar$ values. Therefore, by reflecting topological attributes of the system, $\mathcal{C}\hbar$ remains distinct and irreplaceable.

As the analogy with Gauss's law suggests, a concrete understanding of the phases can be obtained by considering how the singularities of the system move in the parameter space. Given the relatively small size of the Hilbert space, analytic solutions can be obtained and the phase diagram can be predicted by calculating when points with degenerate ground states cross the spherical manifold. The points of ground-state degeneracy are located on the z axis of \mathbf{H}_r space. In Fig. 4c, the small diagrams at right (A, B and C) correspond to the dots labelled A, B and C on the main panel, where g is small. In this limit, H_0 affects only one qubit, and increasing it moves only one monopole past the surface (C). For D, E and F where instead H_0 is small, increasing g further the monopole separation, eventually moving both monopoles outside the surface (F). The results of a full analytical study are plotted in Fig. 4b, which shows three distinct regions and their phase boundaries. There is a direct 0-to-2 transition when $H_0 = 0$, but at finite values the system first goes through the green $\mathcal{C}\hbar = 1$ region. This latter behaviour is seen in Fig. 4c. The dashed lines in Fig. 4a, c are from this analytic solution, which uses no free parameters, and are in good agreement with the measurements. The deviations are mainly systematic errors, due to crosstalk between simultaneous control pulses.

The generality of our method is aligned with Feynman's original idea of quantum simulation²⁴, where a controllable quantum system is used to investigate otherwise inaccessible quantum phenomena. In the absence of other experimental approaches, the full controllability of our superconducting circuits will provide a unique platform for the exploration

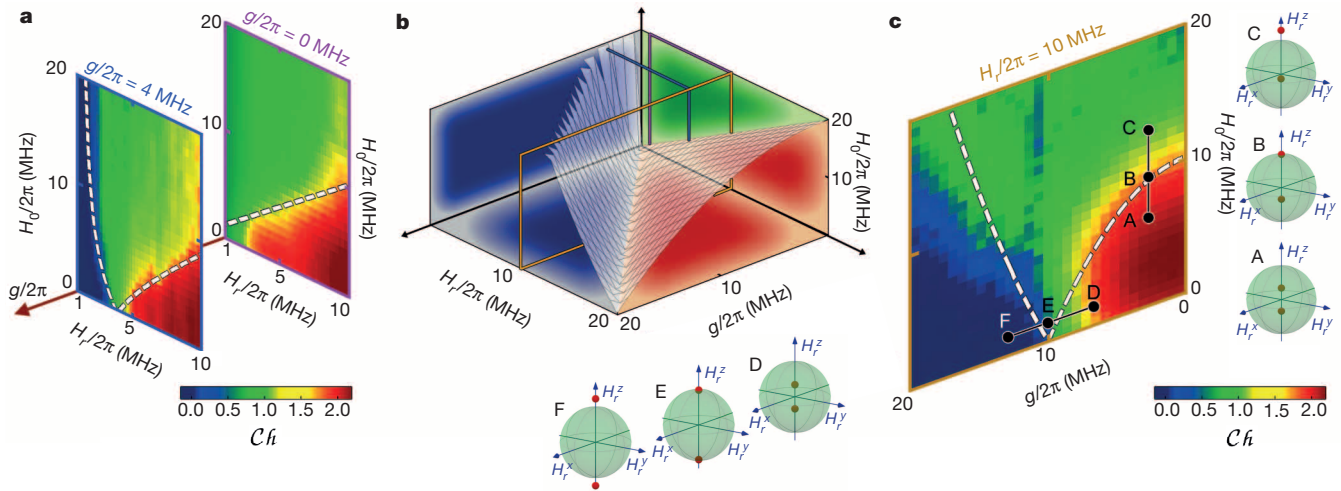


Figure 4 | Topological phase diagram of an interacting system. **a–c**, Measured **(a, c)** and calculated **(b)** phase diagrams of main text equation (5). In **a**, $\mathcal{C}h$ was measured for two fixed $g/2\pi$ values of 4 MHz (left) and 0 MHz (right); in **c**, $\mathcal{C}h$ was measured for fixed $H_x/2\pi = 10$ MHz. Dashed lines are topological transitions calculated analytically. **b**, The analytically

of topological phases of more complex quantum systems, perhaps most notably interacting spin systems where tantalizing evidence for fractionalization has been found⁶. Larger spin systems have smaller energy gaps, and longer ramps will be needed to remain close to the ground-state manifold. A path forward is therefore to improve coherence in multi-qubit systems, research which is currently underway.

Received 24 June; accepted 23 September 2014.

1. Klitzing, K. v., Dorda, G. & Pepper, M. New method for high-accuracy determination of the fine-structure constant based on quantized Hall resistance. *Phys. Rev. Lett.* **45**, 494–497 (1980).
2. Tsui, D. C., Stormer, H. L. & Gossard, A. C. Two-dimensional magnetotransport in the extreme quantum limit. *Phys. Rev. Lett.* **48**, 1559–1562 (1982).
3. Bernevig, B. A., Hughes, T. L. & Zhang, S.-C. Quantum spin Hall effect and topological phase transition in HgTe quantum wells. *Science* **314**, 1757–1761 (2006).
4. Hasan, M. Z. & Kane, C. L. Colloquium: topological insulators. *Rev. Mod. Phys.* **82**, 3045–3067 (2010).
5. Moore, J. E. The birth of topological insulators. *Nature* **464**, 194–198 (2010).
6. Gritsev, V. & Polkovnikov, A. Dynamical quantum Hall effect in the parameter space. *Proc. Natl Acad. Sci. USA* **109**, 6457–6462 (2012).
7. Haldane, F. D. M. Model for a quantum Hall effect without Landau levels: condensed-matter realization of the “parity anomaly”. *Phys. Rev. Lett.* **61**, 2015–2018 (1988).
8. Geller, M. *et al.* Tunable coupler for superconducting Xmon qubits: perturbative nonlinear model. Preprint at <http://arXiv.org/abs/1405.1915> (2014).
9. Chen, Y. *et al.* Qubit architecture with high coherence and fast tunable coupling. Preprint at <http://arXiv.org/abs/1402.7367> (2014).
10. Thouless, D. J., Kohmoto, M., Nightingale, M. P. & den Nijs, M. Quantized Hall conductance in a two-dimensional periodic potential. *Phys. Rev. Lett.* **49**, 405–408 (1982).
11. Wen, X.-G. *Quantum Field Theory of Many-body Systems* (Oxford Univ. Press, 2004).
12. Bernevig, B. A. & Hughes, T. L. *Topological Insulators and Topological Superconductors* (Princeton Univ. Press, 2013).
13. Berry, M. V. Quantal phase factors accompanying adiabatic changes. *Proc. R. Soc. Lond. A* **392**, 45–57 (1984).
14. Wilczek, F. & Shapere, A. *Geometric Phases in Physics* (World Scientific, 1989).

calculated phase diagram showing three distinct $\mathcal{C}h$ volumes and the separatrix plane. The phase diagram cuts in **a** and **c** are indicated by coloured slices. In **c**, the six spheres show the positions of the monopoles in H -space at the indicated locations A–F in the phase diagram of **c**, with radius equalling the fixed $H_x/2\pi = 10$ MHz.

15. Neeley, M. *et al.* Emulation of a quantum spin with a superconducting phase qubit. *Science* **325**, 722–725 (2009).
16. Leek, P. J. *et al.* Observation of Berry’s phase in a solid-state qubit. *Science* **318**, 1889–1892 (2007).
17. Atala, M. *et al.* Direct measurement of the Zak phase in topological Bloch bands. *Nature Phys.* **9**, 795–800 (2013).
18. Mariani, M. *et al.* Implementing the quantum von Neumann architecture with superconducting circuits. *Science* **334**, 61–65 (2011).
19. Houck, A. A., Türeci, H. E. & Koch, J. On-chip quantum simulation with superconducting circuits. *Nature Phys.* **8**, 292–299 (2012).
20. Buluta, I. & Nori, F. Quantum simulators. *Science* **326**, 108–111 (2009).
21. Barends, R. *et al.* Coherent Josephson qubit suitable for scalable quantum integrated circuits. *Phys. Rev. Lett.* **111**, 080502 (2013).
22. Schroer, M. D. *et al.* Measuring a topological transition in an artificial spin-1/2 system. *Phys. Rev. Lett.* **113**, 050402 (2014).
23. Xu, C., Poudel, A. & Vavilov, M. G. Nonadiabatic dynamics of a slowly driven dissipative two-level system. *Phys. Rev. A* **89**, 052102 (2014).
24. Feynman, R. P. Simulating physics with computers. *Int. J. Theor. Phys.* **21**, 467–488 (1982).

Supplementary Information is available in the online version of the paper.

Acknowledgements We acknowledge discussions with J. Moore, C. Nayak, M. Niu, A. Rahmani, T. Souza, M. Vavilov, D. Weld and A. Yazdani. This work was supported by the NSF (grants DMR-0907039 and DMR-1029764), the AFOSR (FA9550-10-1-0110), and the ODNI, IARPA, through ARO grant W911NF-10-1-0334. Devices were made at the UCSB Nanofab Facility, part of the NSF-funded NNIN, and the NanoStructures Cleanroom Facility.

Author Contributions P.R., C.N. and Y.C. designed and fabricated the sample, performed the experiment, analysed the data, and with M.K. and C.Q. co-wrote the manuscript and Supplementary Information. M.K. and A.P. provided theoretical assistance. All members of the UCSB team contributed to the experimental set-up. All authors contributed to the manuscript preparation.

Author Information Reprints and permissions information is available at www.nature.com/reprints. The authors declare no competing financial interests. Readers are welcome to comment on the online version of the paper. Correspondence and requests for materials should be addressed to J.M.M. (martinis@physics.ucsb.edu).